

Direct Measurement of Single-Molecule Adenosine Triphosphatase Hydrolysis Dynamics

Jie Li,^{†,‡} Gen He,^{†,‡} Ueno Hiroshi,[§] Wenzhe Liu,[‡] Hiroyuki Noji,[§] Chuanmin Qi,^{*,†} and Xuefeng Guo^{*,‡,||}

[†]Key Laboratory of Radiopharmaceuticals, Ministry of Education, College of Chemistry, Beijing Normal University, Beijing 100875, P. R. China

[‡]Beijing National Laboratory for Molecular Sciences, State Key Laboratory for Structural Chemistry of Unstable and Stable Species, College of Chemistry and Molecular Engineering, Peking University, Beijing 100871, P. R. China

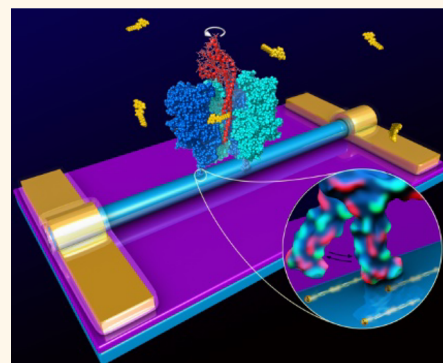
[§]Department of Applied Chemistry, School of Engineering, The University of Tokyo, Tokyo 113-8654, Japan

^{||}Department of Materials Science and Engineering, College of Engineering, Peking University, Beijing 100871, P. R. China

Supporting Information

ABSTRACT: F_1 -ATPase (F_1) is a bidirectional molecular motor that hydrolyzes nearly all ATPs to fuel the cellular processes. Optical observation of labeled F_1 rotation against the $\alpha_3\beta_3$ hexamer ring revealed the sequential mechanical rotation steps corresponding to ATP binding/ADP release and ATP hydrolysis/Pi release. These substeps originate from the F_1 rotation but with heavy load on the γ shaft due to fluorescent labeling and the photophysical limitation of an optical microscope, which hampers better understanding of the intrinsic kinetic behavior of ATP hydrolysis. In this work, we present a method capable of electrically monitoring ATP hydrolysis of a single label-free F_1 in real time by using a high-gain silicon nanowire-based field-effect transistor circuit. We reproducibly observe the regular current signal fluctuations with two distinct levels, which are induced by the binding dwell and the catalytic dwell, respectively, in both concentration- and temperature-dependent experiments. In comparison with labeled F_1 , the hydrolysis rate of nonlabeled F_1 used in this study is 1 order of magnitude faster ($1.69 \times 10^8 \text{ M}^{-1} \text{ s}^{-1}$ at 20°C), and the differences between two sequential catalytic rates are clearer, demonstrating the ability of nanowire nanocircuits to directly probe the intrinsic dynamic processes of the biological activities with single-molecule/single-event sensitivity. This approach is complementary to traditional optical methods, offering endless opportunities to unravel molecular mechanisms of a variety of dynamic biosystems under realistic physiological conditions.

KEYWORDS: silicon nanowires, field-effect transistors, biosensors, F_1 -ATPase, single-molecule dynamics



As the key subcomplex of F_0F_1 -ATPase, F_1 -ATPase ($\alpha_3\beta_3\gamma$, F_1), whose structure directly correlates to its enzymatic function, behaves as the rotary molecular motor.¹ In the whole function of F_0F_1 -ATPase, F_1 is mainly responsible for ATP synthesis/hydrolysis. ATP hydrolysis can drive the γ shaft to periodically rotate against the surrounding $\alpha_3\beta_3$ hexamer, where the α and β subunits are arranged in an alternating pattern. This pattern forms a hexamer ring as the motor's stator, and the central shaft of γ acts as the rotor. The γ rotation leads to either ATP hydrolysis or ATP synthesis, depending on its rotation direction relative to the $\alpha_3\beta_3$ hexamer ring.² The crystallographic structural analysis demonstrated that F_1 has three active catalytic sites located in three β subunits. This has been first proved by direct observation that the F_1 rotor, which has a $2.9 \mu\text{m}$ long microfilament immobilized on γ ,

pauses at each 120° under an optical microscope.³ Tracking F_1 rotations as a function of time by using single-molecule FRET or attaching a nanoscale sphere to the γ rotor with high temporal and angular resolution revealed more details about the F_1 hydrolysis reaction scheme.^{4–8} They found that the 120° step can be divided into 80° and 40° substeps at a certain temperature and ATP concentration,⁹ mainly triggered by ATP binding/ADP release and ATP hydrolysis/Pi release, respectively. To dissect a single complete F_1 power stroke, another study by using a 200 nm golden nanorod labeled on γ as a

Received: October 28, 2017

Accepted: December 7, 2017

Published: December 7, 2017

signal probe with 5 μs time resolution¹⁰ indicated that the accelerations and decelerations occurred during the rotation power stroke of γ , showing the low enzymatic efficiency of direct conversion of ATP chemical energy to mechanical work. In brief, ATP hydrolysis includes four elementary reaction steps: ATP binding, ADP release, ATP hydrolysis, and Pi release.

Although the mechanical rotation and ATP hydrolysis mechanisms of F_1 have been well studied and some kinetic parameters have been detected in a variety of conditions, most of these results came from F_1 containing tens or hundreds of times larger labels on the γ shaft in order to overcome the photophysical limitation of an optical microscope.^{2,3,5,9,11–15} The larger label probe amplifies the optical signal as well as the viscous friction, which hampers the full-speed rotation of γ . In particular, the non-uniform viscous effects under different conditions would vary the temperature and concentration dependence of the F_1 rotary conformation changes, as demonstrated by the fact that previous works with different labels^{3,5,10,15–17} have shown obvious hydrolysis rate or rotation rate discrepancies of F_1 . To solve this challenge, here we present an approach that is able to realize label-free, real-time electrical monitoring of ATP hydrolysis by using a high-gain silicon nanowire (SiNW)-based field-effect transistor (FET) circuit (Figure 1a,b) with high signal-to-noise ratio and time

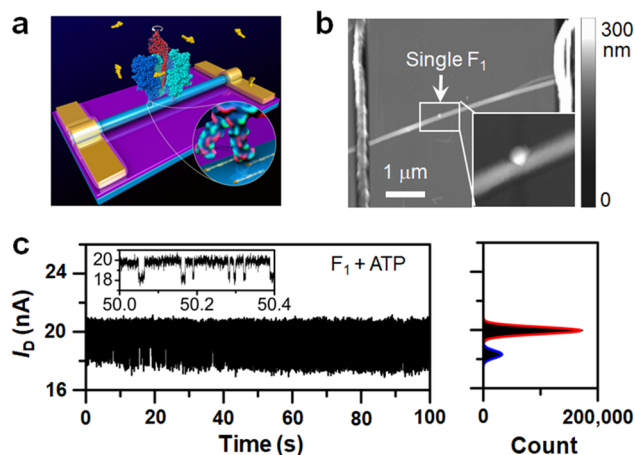


Figure 1. Device structure and electrical characterization of a single F_1 -modified SiNW FET biosensor. (a) Schematic representation of a single F_1 -modified SiNW FET nanocircuit. (b) AFM image showing the success of immobilizing a single F_1 on the silicon nanowire surface. (c) Real-time current recordings of F_1 hydrolysis (10 $^{\circ}\text{C}$, 1 μM ATP). The right panel is the corresponding histogram of current values, showing a bimodal current distribution. The source–drain voltage (V_D) is 0.1 V, and the gate voltage (V_G) is 0.1 V.

resolution. Particularly relevant to our design are the studies of Lieber, Collins, and their co-workers which demonstrated highly sensitive biodetection by using 1D SiNW or carbon nanotube-based FETs.^{18–22} When F_1 hydrolyzes ATP on the surface of the nanowire, the conformational changes of negative-charged F_1 act as a variable local gate, synchronously electrostatically gating the carrier density inside the nanowire and periodically generating current oscillation signals.^{23,24} We have investigated both ATP concentration and temperature dependences of the hydrolysis behaviors of F_1 -ATPase ($\alpha(\text{His}_6$ at N-terminal/C193S) $_3\beta(\text{His}_{10}$ at N-terminal) $_3\gamma(\text{S108C/$

I211C) from thermophilic *bacillus* PS3²⁵). On the basis of electrical measurements, we found that the F_1 hydrolysis rate versus ATP concentration curve is in accordance with the Michaelis–Menten equation with the highest hydrolysis rate of $1.69 \times 10^8 \text{ M}^{-1} \text{ s}^{-1}$ at 20 $^{\circ}\text{C}$, much higher than labeled F_1 reported before.¹⁵

RESULTS AND DISCUSSION

Details of the SiNW synthesis, device fabrication, and modification method can be found in the [Supporting Information](#). By using our previous work of the single protein detection method for single F_1 -ATPase modification,²⁶ the bare devices were immersed in a 10-mM tris-buffer solution (10 mM tris-HCl, 27.6 mM NaCl, 0.54 mM KCl, pH = 8.0, Sigma-Aldrich) with 2 mM MgCl_2 and tested to stabilize the current for at least 5 min as control experiments. After stabilization, we anchored only one F_1 on the sensitive surface of SiNWs by dropping a diluted F_1 solution (100 nM) on Ni-NTA-functionalized SiNW FETs and monitoring the current. The negative-charged F_1 in the tris-buffer solution (pH = 8) caused a current stepwise increase when F_1 individually complexed with the Ni-NTA probe on the nanowire surface (Figure S5). To avoid multiple F_1 adsorption on the surface, washing the devices immediately after the first current increase step appeared was necessary. The F_1 -immobilized devices showed a higher steady conductance in a pure buffer solution. Interestingly, the addition of ATP into the solution (10 $^{\circ}\text{C}$, 1 μM ATP) induced the real-time current fluctuation between two distinct levels (Figure 1c). The gradual increase of the current oscillation frequency indicated the slow starting process of F_1 hydrolysis (also see Figure 2c). To fully reveal the dynamics of F_1 hydrolysis, ATP concentration-/temperature-dependent experiments have been systematically carried out, which will be described in detail in the following section. To further confirm the success of attaching a single F_1 on the surface of a SiNW, we measured the surface morphology of the device by atomic force microscopy (AFM, Dimension Icon, Bruker) after electrical measurement. As shown in Figure 1b, only a single F_1 (~ 12.1 nm including a ~ 2.0 nm linkage)²¹ was detected on the surface of the SiNW (~ 64.3 nm) that nicely spanned source and drain electrodes.

As described above, control experiments by using both the bare device and the F_1 -modified one but in the absence of ATP (Figure 2a,b) demonstrated that the current oscillation happened only with ATP stimulation (Figure 2c). Frequency domain measurements have been used to study the dynamics of the biomolecule-nanowire FET hybrid system.²⁷ The power spectra of real-time $I(t)$ signals in Figure 2d,e (without ATP-induced biomolecule–nanowire dynamic interactions) shown a pure $1/f$ shape. In contrast, the frequency domain spectrum of ATP-present F_1 -immobilized device (Figure 2f) showed a Lorentzian peak superimposed on its $1/f$ shape, indicating a different interaction process. This clearly demonstrated that the ATP-initiated F_1 hydrolysis rotation induced the bistable current signal oscillation.

Figure 3 elaborates all the current versus time data of F_1 hydrolysis under different ATP concentrations (Figure 3a,e) and temperatures (Figure 3f,j) with the base current subtracted to show the pure current oscillation caused by F_1 catalytic hydrolysis. Insets in each left panel are the enlarged view (0.5 s) to display more details of the current signals. Consistently, all the behaviors of F_1 hydrolysis under different conditions showed the two-level current distribution. As a symmetric

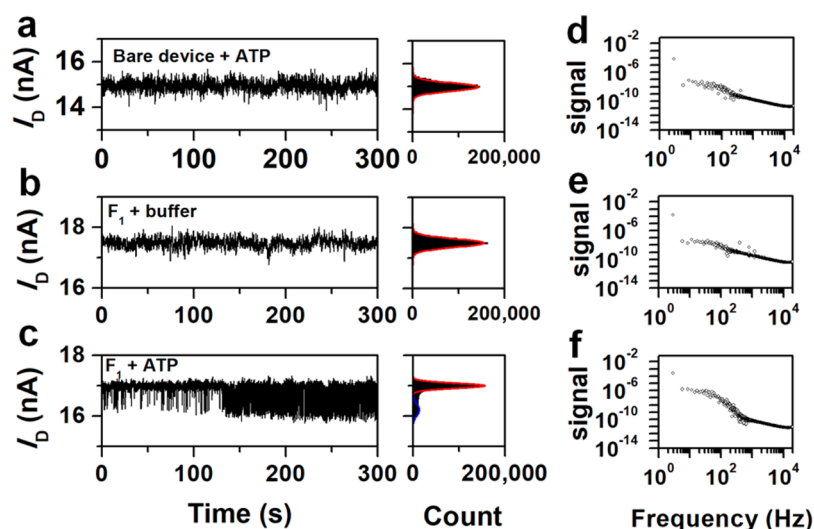


Figure 2. Frequency spectral comparison of control experiments. (a) Real-time monitoring and corresponding current histogram of a bare device under an ATP solution (10 °C, 1 μM ATP). (b) Real-time monitoring and corresponding current histogram of a single F_1 -modified device under a buffer solution. (c) Real-time monitoring and corresponding current histogram of a F_1 -modified device in the presence of ATP (10 °C, 1 μM ATP). (d–f) Corresponding frequency spectra (y -axis unit is V^2/Hz). $V_D = 0.1$ V, $V_G = 0.1$ V.

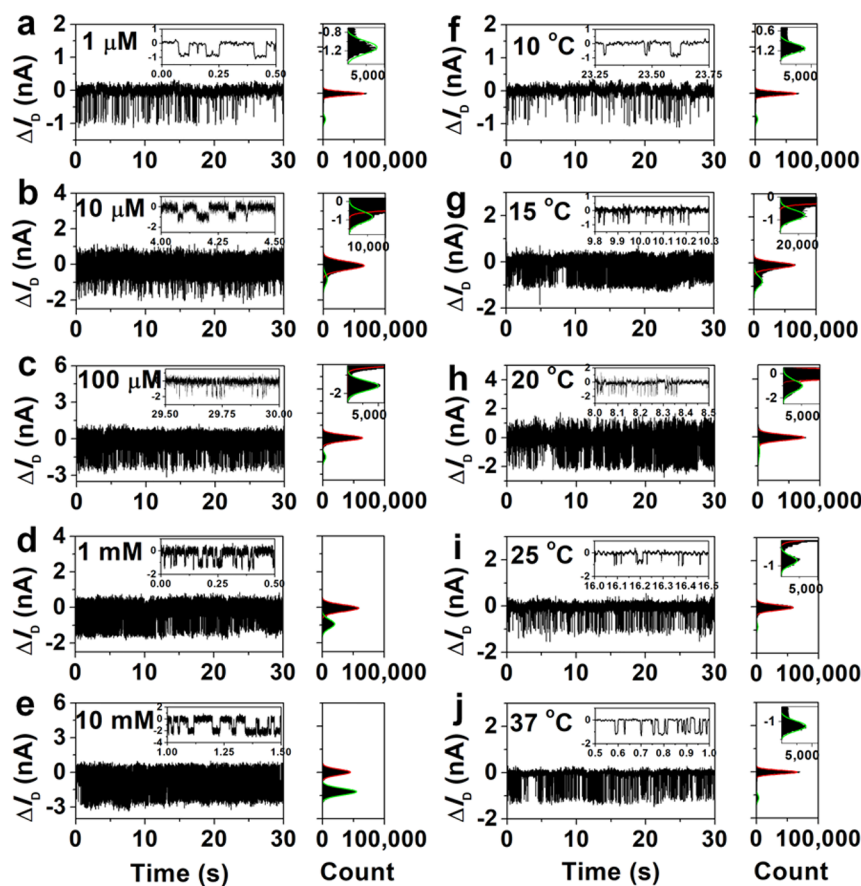


Figure 3. Concentration- and temperature-dependent experiments of F_1 hydrolysis. (a–e) $\Delta I_D(t)$ signals of a single F_1 -modified SiNW FET nanocircuit with different ATP concentrations: (a) 1 μM , (b) 10 μM , (c) 100 μM , (d) 1 mM, (e) 10 mM) at fixed 10 °C and their corresponding current histograms. Insets in $\Delta I_D(t)$ curves show the 0.5 s enlarged view. Insets in the histograms amplify the details of the current distributions. (f–j) $\Delta I_D(t)$ signals of a single F_1 -modified SiNW FET nanocircuit under different temperatures: (f) 10 °C, (g) 15 °C, (h) 20 °C, (i) 25 °C, (j) 37 °C with constant 1 μM ATP and their corresponding current histograms. Insets in $\Delta I_D(t)$ curves show the 0.5 s enlarged view. Insets in the histograms amplify the details of the current distributions. $V_D = 0.1$ V, $V_G = 0.1$ V.

hexamer ring is formed by $\alpha_3\beta_3$, the three heterogeneous catalytic sites of F_1 , commonly designated as β_{TP} (liganded with

MgAMP-PNP), β_{DP} (liganded with Mg-ADP), and β_E (empty), exist in the interface of α and β subunits. β_{TP} and β_{DP} are in

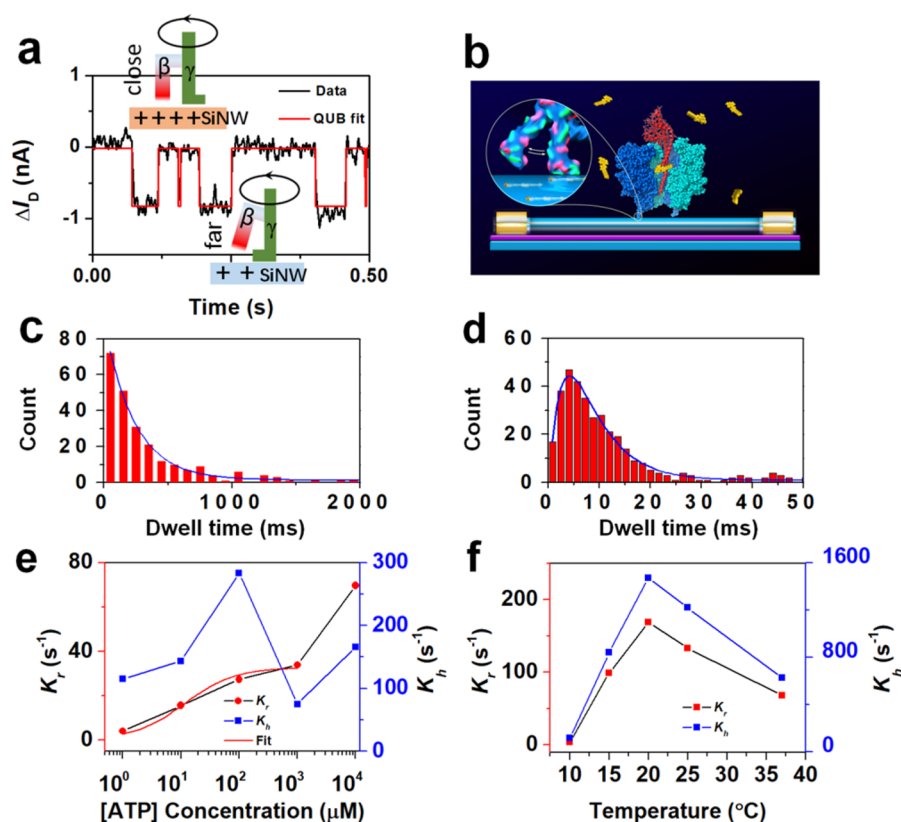


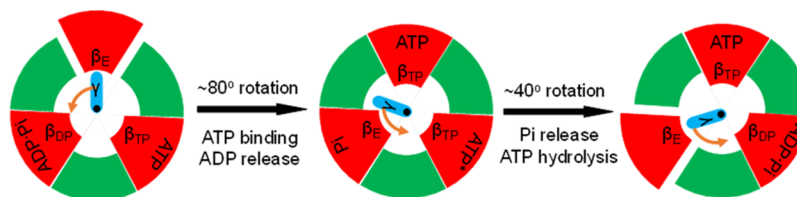
Figure 4. Statistical analysis of F_1 hydrolysis. (a) 0.5 s enlarged view of $\Delta I_b(t)$ signals (black) and QUB fitting (red) from Figure 3a. Insets show β different conformations corresponding to high and low conductive states, respectively. (b) Side view of the device structure, showing how F_1 modulates the property of SiNWs. (c,d) The distribution of the dwell times for high (c) and low (d) current states. (e,f) ATP concentration (e) and temperature (f) dependence of the F_1 hydrolysis rate (blue) and pure catalytic rate (red).

closed conformations, whereas β_E is in an open conformation.²⁸ In our case, F_1 specifically chelated with Ni-NTA on the nanowire surface by His-tags on three β units. So the negative charge-dominated projecting terminals were closest to the surface of SiNWs within the Debye length (~ 4 nm) (10 mM tris-buffer). It is known that the β subunit lever domain is positioned to push against the γ -foot and γ -coiled-coil as it opens and closes, respectively.¹⁰ The γ shaft rotation forces the β subunit conformation to swing back and forth between open and closed states during the ATP hydrolysis process (Figure 1a).⁵ The distance change between the charged N-terminals (possibly in combination with the remote C-terminals) and the nanowire surface equals to a variational molecular gate to the nanocircuit surface capacitance. According to the principle of the p-type silicon nanowire platform, the action of β subunits away from the surface of SiNWs leads to a decrease of the negative gate voltage,²⁹ thus decreasing the hole carrier density inside conductive SiNWs (Figure 4a, bottom inset). Therefore, the high current state corresponds to the F_1 binding dwell (β close to SiNWs), while the low current state is the F_1 catalytic dwell (β far from SiNWs). The relative β conformations and corresponding current states were schematic in Figure 4a,b. We tested more than 53 devices, and 32 of them showed the observed bistable current oscillation, proving the reproducibility.

As shown in Figure 3, the high current state occupies the vast majority of the F_1 hydrolysis time except the oversaturated 10 mM concentration of ATP, consistent with previous consensus that the ATP-binding waiting dwell or inactive state dominates the catalysis process of F_1 .¹⁵ As the hydrolysis process is very

similar to the case of FRET, we used a QUB software, which is widely used to analyze single-molecule fluorescent signals, to extract the dwell time of different current states (Figure 4a, red line).³⁰ Figure 4c,d corresponds to the dwell-time distributions of the high and low current states (10 °C, 1 μ M ATP), respectively. Clearly, the average dwell time of the high state is much longer as ATP-binding waiting dwell dominates the F_1 hydrolysis process.¹⁵ The distribution of the high state exhibits a single exponential behavior with an average dwell-time (τ_0) of ~ 237.44 ms, while the low current state exhibits a biexponential behavior, implying a consecutive two-step reaction. By assuming the consecutive reaction with two time constants, we fitted the dwell-time distribution of the low state with an equation: $A1 \times \exp(-t/\tau_1) - A2 \times \exp(-t/\tau_2)$. This fitting leads to the two time constants of $\tau_1 = \sim 5.99$ ms and $\tau_2 = \sim 2.71$ ms, both of which are much faster than that of the high current process. As reported by the optical observation, the F_1 catalytic process included two main sequential actions: ATP hydrolysis and Pi release.⁹ Correspondingly, the biexponential behaviors of the current pulse should be ascribed to these two motions, respectively: ATP hydrolysis is relatively slower and Pi release is faster according to previous reports.^{8,16}

To further explore the ATP concentration dependence of F_1 hydrolysis, we have analyzed the series of ATP concentrations at 10 °C. As shown in Figure 3a–e from superlow 1 μ M to oversaturated 10 mM ATP, all the current signals exhibited reproducible bistable oscillation characteristics. On the basis of all the dwell times extracted from high and low current states of each concentration, the distribution characteristics of high and low states (Figure S6) were consistent with the case of 1 μ M

Scheme 1. F₁ Catalytic Hydrolysis Path

ATP in Figure 4c,d. The average apparent hydrolysis rate, defined as $k_h = 1/(\tau_0 + \tau_1 + \tau_2)$, increased rapidly with increasing ATP concentrations, from $\sim 4.06 \text{ s}^{-1}$ at $1 \mu\text{M}$ to $\sim 69.74 \text{ s}^{-1}$ at 10 mM . Note that the F₁ catalytic rate, defined as $k_r = 1/(\tau_1 + \tau_2)$, should exclude the ATP-binding waiting dwell time of τ_0 . The highest k_r reached $\sim 283.29 \text{ s}^{-1}$ at $100 \mu\text{M}$. We summarized the kinetic parameters in Table S1 and plotted these two rates as a function of ATP concentration in Figure 4e. It is reasonable to conclude that the increase of ATP concentrations decreases the rate-dominating waiting dwell time and thus increases the apparent hydrolysis rate k_h . Although the catalytic reaction of F₁ is almost independent of ATP concentration, the oversaturated ATP concentration may disturb the programmed rotation and disorder the catalytic rate k_r from the optimum concentration.³¹ This can explain the different concentration-dependent behaviors of k_h and k_r shown in Figure 4e. It is worthwhile to mention that the average apparent hydrolysis rate fits the Michaelis–Menten equation ($V = V_{\text{max}}[\text{ATP}]/(K_m + [\text{ATP}])$) under 1 mM ATP, where V_{max} is the maximum rate and K_m is the ATP concentration at which the reaction rate is half of V_{max} . The corresponding V_{max} and K_m values of F₁ hydrolysis achieved at $10 \text{ }^\circ\text{C}$ are $\sim 32.66 \text{ s}^{-1}$ and $\sim 11.36 \mu\text{M}$, respectively. Importantly, these values are much faster than previous works,^{32,33} thus proving that the label-free F₁ possesses the higher catalytic activity. In addition, the occupancy of catalytic dwell also increased from $\sim 5.3\%$ at $1 \mu\text{M}$ to $\sim 58.8\%$ at 10 mM with increasing the ATP concentration, apparently due to the decrease of the ATP-binding waiting dwell time.

Temperature is another important factor affecting the activity of F₁ hydrolysis. We have measured another 4 different temperatures ($15 \text{ }^\circ\text{C}$, $20 \text{ }^\circ\text{C}$, $25 \text{ }^\circ\text{C}$, and $37 \text{ }^\circ\text{C}$) under a fixed $1 \mu\text{M}$ ATP concentration. Figure 3f–j shows the current oscillation characteristics, again with two distinct levels. Similarly, Figure S7 shows the lifetime distributions of their high and low states by extracting the dwell times of each state. The kinetic parameters of the temperature dependence are summarized in Table S2, by which we plotted the curves of the apparent hydrolysis rate k_h and the F₁ catalytic rate k_r as a function of temperature as shown in Figure 4f. Both k_h and k_r reached the highest rate at $20 \text{ }^\circ\text{C}$. This is consistent with the activity characteristic of F₁ according to a well-described model F₁ from thermophilic *Bacillus* that has two optimum temperatures at 20 and $75 \text{ }^\circ\text{C}$.¹⁵ As reported before,²⁹ because the temperature-sensitive reaction (most probably ADP release step) affects the rate of overall reaction in the F₁ rotation hydrolysis, the rate changed more irregularly at relative high temperatures. The catalytic rate k_r (blue in Figure 4f) exhibits a similar variation tendency with temperature since the continuum of the F₁ catalytic hydrolysis path obeys an exact reaction sequence as shown in Scheme 1. The unreleased ADP or Pi occupies the catalytic site and inhibits next ATP binding, resulting in hydrolysis disorder or even stop (inactive). On the basis of

Table S2, we conclude both the binding dwell and catalytic dwell occupancies are not simply linear with temperature in this temperature range. The highest catalytic rate obtained here is $\sim 168.92 \text{ s}^{-1}$ at $20 \text{ }^\circ\text{C}$ and $1 \mu\text{M}$ ATP concentration with a very low rotary occupancy (7.6%), demonstrating that F₁ has a faster hydrolysis rate with a shorter waiting dwell time or inactive stage (τ_0) since the nonhydrolysis or random inactive stage (τ_0) is the rate-dominating step.

In fact, the irregular changes of the rotary rate may result from the stochastic variation of the F₁ catalysis activity. The non-uniformity of the current pulse frequency randomly happened not only on the initiation stage (Figure 2c) but also existed in the whole hydrolysis process, even under a constant temperature and ATP concentration. Figure 5a shows

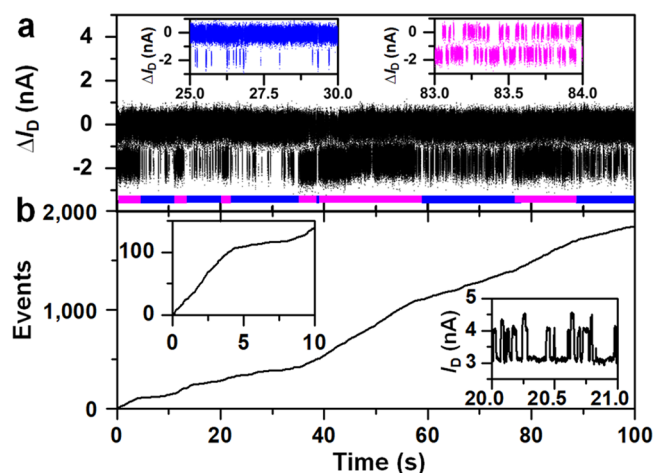


Figure 5. Non-uniform hydrolysis processes of F₁ hydrolysis. (a) A set of current oscillation signals of F₁ hydrolysis. Inset panels are a 1 s enlarged view of slow oscillation signals (blue) and fast oscillation signals (pink). Bottom color bar corresponds to the slow (blue section) and fast (pink section) hydrolysis regions ($10 \text{ }^\circ\text{C}$, $100 \mu\text{M}$ ATP). (b) Hydrolysis events versus time curve. Left inset is the first 10 s enlarged view. Right inset shows the representative three-level current signal fluctuation possibly due to the attachment of two F₁ proteins ($10 \text{ }^\circ\text{C}$, $1 \mu\text{M}$ ATP). $V_D = 0.1 \text{ V}$, $V_G = 0.1 \text{ V}$.

the real-time variation of the current pulses in a longtime scale. The fast and slow hydrolysis stages are randomly alternated (marked with blue and pink ribbons in Figure 5a, respectively). To clearly show the variation of the hydrolysis rate, we extracted out the pulse signals to plot a hydrolysis events versus time curve in Figure 5b. This phenomenon has been frequently seen in the time courses of F₁ rotation in previous works.⁸ The hydrolysis events remain unchanged for a relative long time frequently, representing the inactivation of F₁ hydrolysis,¹⁴ due to many reasons such as Mg-ADP inhibition or Pi rebinding.³⁴ Note that in single-molecule experiments, the time-average value is equivalent to the ensemble average in ensemble experiments, where the differences from individual behaviors

are overlapped among many molecules. In the current case of single-molecule electrical detection, we are able to probe the subtle details of the hydrolysis events of a single F_1 with high time resolution. The hydrolysis rate *versus* time curve displays the non-uniformity of the catalytic rate or rotation rate of the γ shaft. In addition, the time width of the current pulse varies in the range from tens of microseconds to tens of milliseconds. To clearly show the differences, the enlarged views with low and high pulse frequencies are represented in Figure 5a, insets. The understanding of intrinsic molecular mechanisms and the discovery of new effects of F_0F_1 -ATPase activities at the single-molecule/single-event level by taking advantage of these huge details deserve further research. It should be mentioned that we sometimes observed the three-level current signal fluctuation in real-time measurements (Figure 5b, right inset and Figure S8), which probably results from the superimposed behavior of additional F_1 that was attached on or close to the SiNW surface.

CONCLUSION

In this study, we demonstrate a single-molecule electrical detection approach that is able to realize label-free, real-time electrical monitoring of the dynamic process of F_1 hydrolysis at the single-molecule/single-event level, by using ultrasensitive SiNW FET nanocircuits. We observed the reproducible large-amplitude two-level current fluctuations, where the high current state corresponds to the ATP binding dwell (the rate-dominating step) and the low current state originates from two catalytic dwell: ATP hydrolysis and P_i release. ATP concentration-dependent experiments demonstrated a Michaelis–Menten model under 1 mM ATP for F_1 hydrolysis, while temperature-dependent results revealed the intrinsic k_h and k_r at 20 °C, which is an order of magnitude larger than labeled F_1 . These results distinguish this nanocircuit-based architecture as an appropriate platform of single-molecule electrical bio-detection with the advantages, such as label-free capability and single-event sensitivity, providing endless opportunities to probe molecular mechanisms of a variety of dynamic biosystems under realistic physiological conditions, for example, DNA mutation, protein folding, enzymatic activity, and DNA protein interaction.

METHODS

Device Fabrication. Boron-doped p-type SiNWs were synthesized at 465 °C for about 25 min, by using 2.5 sccm disilane (Matheson Gas Products, 99.998% Purity) as the reactant source, 0.11 sccm diborane (100 ppm, diluted in H_2) and 7.5 sccm H_2 as the carrier gas, and 20 nm golden nanoparticles (Ted Pella) as catalysts. The SiNW surfaces were functionalized with N-APTMS (Sigma-Aldrich, 99%) in a vacuum desiccator before transferred to a 1.5 cm \times 1.6 cm silicon substrate. After defining the electrode pattern with a standard UV photolithographic process (UV Exposure machine, BG-401A, China Electronics Technology Group Corporation), 8 nm Cr/80 nm Au were deposited through thermal evaporation (ZHD-300, Beijing Technol Science) to form metal electrodes. Then a 50 nm-thick SiO_2 protective layer was deposited through electron beam thermal evaporation (TEMD-600, Beijing Technol Science) in order to passivate the contact interface. After lift-off with acetone, the amino-functionalized SiNW FET devices were obtained.

Surface Functionalization and Electrical Characterization. The amino-functionalized SiNW FET devices obtained above immediately reacted with *p*-phenylenediisothiocyanate (PDITC 1 mg/mL, Sigma-Aldrich, 99%), followed with 5 mM $N\alpha$, $N\alpha$ -bis(carboxymethyl)-L-lysine hydrate (AB-NTA, Sigma-Aldrich, 99%) reaction and then $NiCl_2$ (5 mM, Sigma-Aldrich, 99.99%) complexation. These sequential reactions provided Ni-NTA end groups for the

following F_1 attachment. Devices characterization was carried out before and after functionalization by using an Agilent 4155C semiconductor analyzer and a Karl Süss (PMS) manual probe station. Figure S3 demonstrated that the SiNW transistors showed a typical p-type behavior with good ohmic contacts. After the multiple functionalization steps, the devices remained at their high sensitivity.

Single F_1 Decoration and Real-Time Electrical Measurements. After device functionalization, we monitored the devices in the buffer solution for several minutes to stabilize the current. Then a 5 μ L diluted F_1 solution (100 nM) was dropped on the device. When the first current step occurred, we immediately washed the devices with excess tris-buffer (5 mL for three times) to avoid excessive F_1 that was possibly noncovalently adsorbed on the surface. This treatment ensured the success of immobilizing only a single F_1 (yield \sim 60%, 32 out of 53).²¹ The single-molecule dynamics measurements in buffer solutions at different temperatures and ATP concentrations were performed with a ziControl program. The electrical currents through selected electrode pairs were collected by using a transimpedance current amplifier (HF2LI lock-in amplifier) at a sampling rate of 28.8 kSa/s by a NIDAQ card, realizing a microsecond time scale. The transimpedance amplifier also set a DC voltage to the source–drain electrodes with a bandwidth filter of 5 kHz (100 nA/V sensitivity). The temperature was precisely controlled with a proportion-integration-differentiation control system and a liquid N_2 cooling system (resolution 0.001 °C; stability better than ± 0.1 °C) on the test stage, which consists of a manual probe station and an INSTEC hot and cold chuck (HCC214S, INSTEC).

ASSOCIATED CONTENT

Supporting Information

The Supporting Information is available free of charge on the ACS Publications website at DOI: 10.1021/acsnano.7b07639.

Additional figures and tables showing device fabrication, surface functionalization, electrical characterization, single F_1 protein decoration, real-time electrical measurement analysis, addition analysis of F_1 hydrolysis, and additional references (PDF)

AUTHOR INFORMATION

Corresponding Authors

*E-mail: guoxf@pku.edu.cn.

*E-mail: qichuanmin@bnu.edu.cn.

ORCID

Xuefeng Guo: 0000-0001-5723-8528

Notes

The authors declare no competing financial interest.

ACKNOWLEDGMENTS

We acknowledge primary financial support from National Key R&D Program of China (2017YFA0204901) and the National Natural Science Foundation of China (grants 21373014 and 21727806).

REFERENCES

- (1) Boyer, P. D.; Cross, R. L.; Momsen, W. A New Concept for Energy Coupling in Oxidative Phosphorylation Based on a Molecular Explanation of the Oxygen Exchange Reactions. *Proc. Natl. Acad. Sci. U. S. A.* **1973**, *70*, 2837–2839.
- (2) Itoh, H.; Takahashi, A.; Adachi, K.; Noji, H.; Yasuda, R.; Yoshida, M.; Kinosita, K. Mechanically Driven ATP Synthesis by F_1 -ATPase. *Nature* **2004**, *427*, 465–468.
- (3) Noji, H.; Yasuda, R.; Yoshida, M.; Kinosita, K. Direct Observation of the Rotation of F_1 -ATPase. *Nature* **1997**, *386*, 299–302.

- (4) Iino, R.; Murakami, T.; Iizuka, S.; Kato-Yamada, Y.; Suzuki, T.; Yoshida, M. Real-Time Monitoring of Conformational Dynamics of the ϵ Subunit in F1-ATPase. *J. Biol. Chem.* **2005**, *280*, 40130–40134.
- (5) Ueno, H.; Suzuki, T.; Kinoshita, K.; Yoshida, M. ATP-Driven Stepwise Rotation of FoF1-ATP Synthase. *Proc. Natl. Acad. Sci. U. S. A.* **2005**, *102*, 1333–1338.
- (6) Okazaki, K.-i.; Hummer, G. Phosphate Release Coupled to Rotary Motion of F1-ATPase. *Proc. Natl. Acad. Sci. U. S. A.* **2013**, *110*, 16468–16473.
- (7) Masaike, T.; Koyama-Horibe, F.; Oiwa, K.; Yoshida, M.; Nishizaka, T. Cooperative Three-step Motions in Catalytic Subunits of F1-ATPase Correlate with 80° and 40° Substep Rotations. *Nat. Struct. Mol. Biol.* **2008**, *15*, 1326–1333.
- (8) Watanabe, R.; Minagawa, Y.; Noji, H. Thermodynamic Analysis of F1-ATPase Rotary Catalysis Using High-Speed Imaging. *Protein Sci.* **2014**, *23*, 1773–1779.
- (9) Yasuda, R.; Noji, H.; Yoshida, M.; Kinoshita, K.; Itoh, H. Resolution of Distinct Rotational Substeps by Submillisecond Kinetic Analysis of F1-ATPase. *Nature* **2001**, *410*, 898–904.
- (10) Martin, J. L.; Ishmukhametov, R.; Hornung, T.; Ahmad, Z.; Frasch, W. D. Anatomy of F1-ATPase Powered Rotation. *Proc. Natl. Acad. Sci. U. S. A.* **2014**, *111*, 3715–20.
- (11) Diez, M.; Zimmermann, B.; Borsch, M.; König, M.; Schweinberger, E.; Steigmiller, S.; Reuter, R.; Felekyan, S.; Kudryavtsev, V.; Seidel, C. A. M.; Graber, P. Proton-Powered Subunit Sotation in Single Membrane-Bound FoF1-ATP Synthase. *Nat. Struct. Mol. Biol.* **2004**, *11*, 135–141.
- (12) Nishizaka, T.; Oiwa, K.; Noji, H.; Kimura, S.; Muneyuki, E.; Yoshida, M.; Kinoshita, K. Chemomechanical Coupling in F1-ATPase Revealed by Simultaneous Observation of Nucleotide Kinetics and Rotation. *Nat. Struct. Mol. Biol.* **2004**, *11*, 142–148.
- (13) Rondelez, Y.; Tresset, G.; Nakashima, T.; Kato-Yamada, Y.; Fujita, H.; Takeuchi, S.; Noji, H. Highly Coupled ATP Synthesis by F1-ATPase Single Molecules. *Nature* **2005**, *433*, 773–777.
- (14) Adachi, K.; Oiwa, K.; Nishizaka, T.; Furuike, S.; Noji, H.; Itoh, H.; Yoshida, M.; Kinoshita, K., Jr Coupling of Rotation and Catalysis in F1-ATPase Revealed by Single-Molecule Imaging and Manipulation. *Cell* **2007**, *130*, 309–321.
- (15) Furuike, S.; Adachi, K.; Sakaki, N.; Shimo-Kon, R.; Itoh, H.; Muneyuki, E.; Yoshida, M.; Kinoshita, K., Jr Temperature Dependence of the Rotation and Hydrolysis Activities of F1-ATPase. *Biophys. J.* **2008**, *95*, 761–770.
- (16) Watanabe, R.; Hayashi, K.; Ueno, H.; Noji, H. Catalysis-Enhancement via Rotary Fluctuation of F1-ATPase. *Biophys. J.* **2013**, *105*, 2385–2391.
- (17) Enoki, S.; Iino, R.; Niitani, Y.; Minagawa, Y.; Tomishige, M.; Noji, H. High-Speed Angle-Resolved Imaging of a Single Gold Nanorod with Microsecond Temporal Resolution and One-Degree Angle Precision. *Anal. Chem.* **2015**, *87*, 2079–2086.
- (18) Cui, Y.; Wei, Q. Q.; Park, H. K.; Lieber, C. M. Nanowire Nanosensors for Highly Sensitive and Selective Detection of Biological and Chemical Species. *Science* **2001**, *293*, 1289–1292.
- (19) Cui, Y.; Zhong, Z.; Wang, D.; Wang, W. U.; Lieber, C. M. High Performance Silicon Nanowire Field Effect Transistors. *Nano Lett.* **2003**, *3*, 149–152.
- (20) Patolsky, F.; Timko, B. P.; Yu, G.; Fang, Y.; Greytak, A. B.; Zheng, G.; Lieber, C. M. Detection, Stimulation, and Inhibition of Neuronal Signals with High-Density Nanowire Transistor Arrays. *Science* **2006**, *313*, 1100–1104.
- (21) Choi, Y. K.; Moody, I. S.; Sims, P. C.; Hunt, S. R.; Corso, B. L.; Perez, I.; Weiss, G. A.; Collins, P. G. Single-Molecule Lysozyme Dynamics Monitored by an Electronic Circuit. *Science* **2012**, *335*, 319–324.
- (22) Sims, P. C.; Moody, I. S.; Choi, Y.; Dong, C.; Iftikhar, M.; Corso, B. L.; Gul, O. T.; Collins, P. G.; Weiss, G. A. Electronic Measurements of Single-Molecule Catalysis by cAMP-Dependent Protein Kinase A. *J. Am. Chem. Soc.* **2013**, *135*, 7861–7868.
- (23) Choi, Y.; Moody, I. S.; Sims, P. C.; Hunt, S. R.; Corso, B. L.; Perez, I.; Weiss, G. A.; Collins, P. G. Single-Molecule Lysozyme Dynamics Monitored by an Electronic Circuit. *Science* **2012**, *335*, 319–324.
- (24) He, G.; Li, J.; Ci, H.; Qi, C.; Guo, X. Direct Measurement of Single-Molecule DNA Hybridization Dynamics with Single-Base Resolution. *Angew. Chem., Int. Ed.* **2016**, *55*, 9036–9040.
- (25) Watanabe, R.; Noji, H. Characterization of the Temperature-Sensitive Reaction of F1-ATPase by Using Single-Molecule Manipulation. *Sci. Rep.* **2015**, *4*, 4962.
- (26) Li, J.; He, G.; Ueno, H.; Jia, C.; Noji, H.; Qi, C.; Guo, X. Direct Real-time Detection of Single Proteins Using Silicon Nanowire-based Electrical Circuits. *Nanoscale* **2016**, *8*, 16172–16176.
- (27) Zheng, G.; Gao, X. P. A.; Lieber, C. M. Frequency Domain Detection of Biomolecules Using Silicon Nanowire Biosensors. *Nano Lett.* **2010**, *10*, 3179–3183.
- (28) Allison, W. S. F1-ATPase: A Molecular Motor That Hydrolyzes ATP with Sequential Opening and Closing of Catalytic Sites Coupled to Rotation of Its γ Subunit. *Acc. Chem. Res.* **1998**, *31*, 819–826.
- (29) Choi, Y.; Olsen, T. J.; Sims, P. C.; Moody, I. S.; Corso, B. L.; Dang, M. N.; Weiss, G. A.; Collins, P. G. Dissecting Single-Molecule Signal Transduction in Carbon Nanotube Circuits with Protein Engineering. *Nano Lett.* **2013**, *13*, 625–31.
- (30) Nicolai, C.; Sachs, F. Solving Ion Channel Kinetics with The QUB Software. *Biophys. Rev. Lett.* **2013**, *08*, 191–211.
- (31) Uchihashi, T.; Iino, R.; Ando, T.; Noji, H. High-Speed Atomic Force Microscopy Reveals Rotary Catalysis of Rotorless F1-ATPase. *Science* **2011**, *333*, 755–758.
- (32) Enoki, S.; Watanabe, R.; Iino, R.; Noji, H. Single-Molecule Study on the Temperature-Sensitive Reaction of F1-ATPase with a Hybrid F1 Carrying a Single b(E190D). *J. Biol. Chem.* **2009**, *284*, 23169–76.
- (33) Shimabukuro, K.; Yasuda, R.; Muneyuki, E.; Hara, K. Y.; Kinoshita, K., Jr.; Yoshida, M. Catalysis and Rotation of F1Motor: Cleavage of ATP at the Catalytic Site Occurs in 1 ms before 40 Degree Substep Rotation. *Proc. Natl. Acad. Sci. U. S. A.* **2003**, *100*, 14731–6.
- (34) Watanabe, R.; Iino, R.; Shimabukuro, K.; Yoshida, M.; Noji, H. Temperature-Sensitive Reaction Intermediate of F1-ATPase. *EMBO Rep.* **2008**, *9*, 84–90.